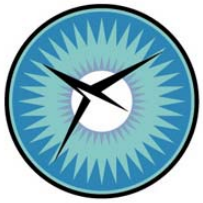

**NATIONAL INSTITUTE OF AEROSPACE**

**Final Report For:**
**NASA # NNL06AC78T**

**Task Title:**
**Updated Results for the Wake Vortex Inverse Model**
**Prepared by:**

Robert E. Robins, David Y. Lai,
Donald P. Delisi, George R. Mellman

**Task Monitor:**
Dr. Fred H. Proctor, NASA Technical Monitor

**Reporting Period:**
**October, 2008**

NWRA NorthWest Research Associates – www.nwra.com

4118 148th Ave NE, Redmond, WA 98052 Tel: 425.556.9055 Fax: 425.556.9099

**NWRA-SEA-08-R368** **3 October 2008**

# Updated Results for the Wake Vortex Inverse Model

By

David Y. Lai, George R. Mellman, Robert E. Robins,
and
Donald P. Delisi

Subcontract TO6-6000-NWRA, Subtask 3.3.2

For
NATIONAL INSTITUTE OF AEROSPACE
Dr. David J. Peake, Vice President of Research and Program Development
100 Exploration Way
Hampton, VA 23666-6147

NASA LANGLEY RESEARCH CENTER
Dr. Fred H. Proctor, NASA Technical Monitor
Hampton, VA 23681

# Table of Contents

## 1. Introduction

NorthWest Research Associates (NWRA) has developed an Inverse Model for inverting aircraft wake vortex data. The objective of the inverse modeling is to obtain estimates of the vortex circulation decay and crosswind vertical profiles, using time history measurements of the lateral and vertical position of aircraft vortices. The Inverse Model performs iterative forward model runs using estimates of vortex parameters, vertical crosswind profiles, and vortex circulation as a function of wake age. Iterations are performed until a user-defined criterion is satisfied. Outputs from an Inverse Model run are the best estimates of the time history of the vortex circulation derived from the observed data, the vertical crosswind profile, and several vortex parameters.

The forward model, named SHRAPA, used in this inverse modeling is a modified version of the Shear-APA model, and it is described in Section 2 of this document. Details of the Inverse Model are presented in Section 3. The Inverse Model was applied to lidar-observed vortex data at three airports: FAA acquired data from San Francisco International Airport (SFO) and Denver International Airport (DEN), and NASA acquired data from Memphis International Airport (MEM). The results are compared with observed data. This Inverse Model validation is documented in Section 4. A summary is given in Section 5. A user's guide for the inverse wake vortex model is presented in a separate NorthWest Research Associates technical report (Lai and Delisi, 2007a).

## 2. Wake Vortex Forward Model

The forward model, SHRAPA, used in this inverse modeling is a modified version of the Shear-APA model (Robins and Delisi, 2006). In this forward model, the vertical and lateral positions of the vortices are computed based on point vortex dynamics. There is also a contribution to changes in lateral position from advection by the crosswind. In addition, SHRAPA includes the effects of vertical wind shear on the evolution of trailing vortices. The observed tilting of a wake vortex pair is attributed to the crosswind shear (or, more precisely, the crosswind shear gradient,) as described below.

In an atmospheric environment without wind shear, an equation for the circulation of a single wake vortex at an age of $t+\Delta t$ is written as

$$\Gamma_{t+\Delta t} = \Gamma_t + \Delta t \frac{d\Gamma_E}{dt} \quad , \qquad (1)$$

where $\Gamma_t$ is the vortex circulation at age t, and $d\Gamma_E/dt$ is the circulation decay rate. The circulation decay rate is defined such that the absolute value of the circulation becomes smaller over time. For a counter-rotating aircraft wake vortex pair, the initial circulations for the port and starboard vortices are negative and positive (the convention used in this forward model), respectively. Therefore, the decay rate, $d\Gamma_E/dt$, has different signs for the port and starboard vortices (in our convention, positive and negative for port and starboard vortices, respectively).

In SHRAPA, we introduce additional circulation changes specifically caused by the vertical shear in the crosswind profile. The rate of change in circulation, $d\Gamma_X/dt$, due to crosswind shear is added to the circulation equation (Eqn. 1) as

$$\Gamma_{t+\Delta t} = \Gamma_t + \Delta t \left( \frac{d\Gamma_E}{dt} + \frac{d\Gamma_X}{dt} \right). \tag{2}$$

To determine $d\Gamma_X/dt$ in terms of the crosswind shear, we note that the vorticity equation for the evolution of axial vorticity ($\eta$) in a trailing vortex can be approximated as

$$\frac{d\eta}{dt} = w \frac{d^2V}{dz^2}, \tag{3}$$

where w is the vertical velocity, V(z) the crosswind vertical profile, and z the vertical coordinate. In the cell formed around a newly generated counter-rotating pair of trailing vortices, w is the descent speed of the cell. Integrating over an area, A, around a vortex within the cell yields

$$\frac{d\Gamma_X}{dt} = \iint_A w \frac{d^2V}{dz^2}, \tag{4}$$

where the axial circulation $\Gamma_X$ is

$$\Gamma_X = \iint_A \eta. \tag{5}$$

Taking the area A to be one-half the area of the cell surrounding a trailing vortex pair yields a parametric model for the rate of change in circulation due to crosswind shear gradient

$$\frac{d\Gamma_X}{dt} = 1.42 b_o^2 w \frac{d^2V}{dz^2}. \tag{6}$$

In this equation, w and $d^2V/dz^2$ (the crosswind shear gradient term) are assumed to be averaged over the half-cell, and, following Greene (1986), the shape of the cell is assumed to be described by an ellipse with semi-axes of length $2.09b_o/2$ and $1.73b_o/2$, where $b_o$ is the elliptic loading value of the initial vortex separation ($\pi/4$ times the aircraft wingspan). Note that immediately after the generation of the vortices, w is constant over the cell, but, as the evolution proceeds, the vortices can tilt, and w can vary over the cell. However, since w and $d^2V/dz^2$ typically change slowly over the cell, w and $d^2V/dz^2$ can be approximated as the values they assume at the center of the vortex cell.

For a given crosswind vertical profile, the crosswind shear gradient can increase or decrease the circulation of a vortex, depending on the sign of the crosswind shear gradient term, $d^2V/dz^2$ (Eqn. 6), and the sign of the circulation decay term, $d\Gamma_E/dt$ (Eqn. 1 and 2). Due to the different signs in the circulation for the port and starboard vortices, the effect of a given crosswind shear gradient on a pair of counter-rotating vortices is to increase the circulation of one vortex and reduce the circulation of the other vortex, relative to their circulations in an unsheared flow. Thus, the crosswind shear gradient results in different circulation strengths for the two vortices over time. These vortices

with different circulation strengths will descend at different speeds, causing the tilting of the vortex pair system.

The inputs for the forward model, SHRAPA, are

(1) the initial lateral position ($y_o$), the initial vertical position ($z_o$), and the initial lateral vortex separation ($b_o$) of the vortex pair,
(2) the vortex circulation as a function of wake age, $\Gamma_E(t)$, and
(3) the crosswind vertical profile, V(z).

The initial vortex circulation, $\Gamma_o$, is given implicitly as $\Gamma_E(0)$. The general circulation decay rate, $d\Gamma_E/dt$, is computed from the input circulation $\Gamma_E(t)$. The change in circulation for each vortex due to the crosswind shear gradient term is computed from the input crosswind profile V(z), using Eqn. 6. The outputs for SHRAPA are model predictions of the lateral position, vertical position, and circulation for both the port and starboard vortices.

## 3. Wake Vortex Inverse Model

The Inverse Model is based on an iterative linearized inversion method which seeks to obtain parameter estimates using forward model predictions that best fit the observed data, subject to smoothness constraints. The forward model used is the SHRAPA code described in Section 2. The observed data used for this Inverse Model are the time evolution of the measured lateral position and vertical position of both the port and starboard aircraft wake vortices. The parameters to be estimated are the initial vortex lateral separation $b_o$, the initial vortex circulation $\Gamma_o$, the initial vortex lateral position $y_o$, the initial vortex vertical position $z_o$, the crosswind vertical profile V(z), and the time history of the vortex circulation $\Gamma(t)$.

The Inverse Model starts with a set of initial guesses for the parameters to be estimated, and performs an iterative forward model run using these parameters. Forward model predictions of lateral transport and altitude are then compared with the observed data. Differences between the data and model predictions guide the choice of vortex parameter values, crosswind profile, and circulation evolution in the next iteration. Iterations are continued in this matter until a user-defined criterion is satisfied. Details of the Inverse Model are described below.

A parameter vector containing all the parameters to be estimated is defined as

$$m = \left[ V(z_1), ..., V(z_k), \Gamma(t_1), ..., \Gamma(t_p), y_o, z_o, b_o \right]. \quad (7)$$

Note that $\Gamma_o$ is just $\Gamma(t)$ at t=0. Forward model predictions using the parameter vector *m* are time histories of the lateral and vertical positions for the port and starboard vortices,

$$d(m) = \left[ y^p(t), ..., y^s(t), z^p(t), ..., z^s(t) \right]. \quad (8)$$

The inverse modeling begins with a starting parameter vector, denoted by $m^0$. The forward model is represented by $d$, and forward model predictions for $m^0$ are denoted by $d(m^0)$. A point perturbation ($\delta m$) is performed for each of the parameters to produce a set of forward model predictions, $d(m^0+\delta m)$. A partial derivative (gradient) matrix, $A$, is formed by

$$A(m^0) = \frac{\partial d}{\partial m}(m^0) \approx \left\{ d\left(m^0 + \delta m\right) - d\left(m^0\right) \right\} \frac{1}{\delta m}. \tag{9}$$

The linearized equation relating a new parameter vector $m = m^0 + \delta m$ to a new set of forward model predictions is

$$d\left(m^0 + \delta m\right) \approx d\left(m^0\right) + A\left(m^0\right)\delta m. \tag{10}$$

Let $D$ be the vector of observations. Then, we wish to find $\delta m$ that minimizes

$$\left\| D - d\left(m^0\right) - A\left(m^0\right)\delta m \right\|, \tag{11}$$

where the least squares (or $L^2$) norm is usually used.

However, this problem is not, in general, well posed. To make the problem well posed, we introduce smoothness constraints on the model, using a system of equations to minimize the second derivatives of V and Γ,

$$\left\| \frac{\partial^2 V}{\partial z^2} \right\| \text{ and } \left\| \frac{\partial^2 \Gamma}{\partial t^2} \right\|. \tag{12}$$

This is achieved by introducing a matrix C

$$C = \begin{pmatrix} A \\ B \end{pmatrix}, \tag{13}$$

where the matrix $B$ has the form

$B$(i,j) = 1 if j = i-1 or i+1
= -2 if j = 1
= 0 otherwise

Rows for the matrix B are formed only for the parameters in $m$ that are not related to the V and Γ parameters. We now solve the equation, in the least square sense,

$$C\left(m^0\right)\delta m = D - d\left(m^0\right) \equiv \delta D. \tag{14}$$

In addition, rows in the matrices $A$ and $B$ can be scaled to provide different weighting for different parameters. The least squares solution, which minimizes

$$w_1^2 \left\| D - d\left(m\right) - A(m^0)\delta m \right\|^2 + w_2^2 \left\| \frac{\partial^2 V}{\partial z^2} \right\|^2 + w_3^2 \left\| \frac{\partial^2 \Gamma}{\partial t^2} \right\|^2 \tag{15}$$

is $$\delta m = \left(C^T C\right)^{-1} C^T \begin{pmatrix} \delta D \\ 0 \end{pmatrix}^T . \quad (16)$$

The weights $w_1$ are for the parameter vector $m$, and can be different for different parameters. The weights $w_2$ and $w_3$ are for the second derivatives of V and Γ, respectively.

In addition, we also introduce constraints to limit the changes in $y_0$, $z_0$, and $b_0$, and the product of $\Gamma_0 b_0$ in the matrix $B$. The additional penalty terms are in the form of

$$w_4^2 \left\| \delta y_o \right\|^2 + w_5^2 \left\| \delta z_o \right\|^2 + w_6 \left\| \delta b_o \right\|^2 + w_7^2 \left\| \delta \Gamma_o b_o + \Gamma_o \delta b_o \right\|^2 . \quad (17)$$

Since the forward problem is not linear, the solution $m=m^0+\delta m$ does not necessarily produce a decrease in the error function. We, therefore, find a scalar $\varepsilon \leq 1$ such that $m=m^0+\varepsilon\delta m$ minimizes the error function. The inherent non-linearity of the forward model requires that the linearized solution be applied iteratively until convergence is achieved. At the end of each iteration, the solved parameter set ($m$) is taken to be the starting parameter set ($m^0$) for the next iteration. The convergence criterion used is that the improvement in the error function falls below a threshold value. For the inversions performed in this study, a threshold change of less than 1 percent was used.

An initial guess for the parameter vector has to be provided for the first inversion iteration. The crosswind profile, V(z), is always taken to be zero in the first iteration. Despite a zero crosswind as the initial guess, the Inverse Model usually converges to a correct crosswind profile after one or two iterations. The initial guess for Γ(t) is taken to be a straight line joining $\Gamma_o$ and the last observed Γ(t). Experiments performed using various Γ(t) indicate that the inversion results are not critically sensitive to the initial choice of Γ(t).

The initial guess of vortex parameters $\Gamma_o$ and $b_o$ used in the Inverse Model are provided by a database. For each aircraft, the initial descent rate, $V_o$, is estimated by linear regression of the observed time history of the vortex vertical positions. From these $V_o$ estimates, $b_o$ and $\Gamma_o$ are computed based on conservation principles (Betz). Details of this analysis and the statistics of the $V_o$ and $b_o$ obtained are described in a separate NorthWest Research Associates technical report (Lai and Delisi, 2007b).

## 4. Wake Vortex Inverse Model Validation

Lidar measurements of lateral and vertical positions of wake vortices generated by landing aircraft in the OGE regions at three airports were used in the Inverse Model. At Memphis International Airport (MEM), the NASA–acquired data were obtained using a continuous wave (CW) lidar. Data from 29 B727 landings and 16 DC9 landings at MEM were used in the Inverse Model. At San Francisco International Airport (SFO) and Denver International Airport (DEN), the FAA-acquired data were collected using a

pulsed lidar. Data from nine aircraft models at SFO and eight aircraft models at DEN were used in the Inverse Model. Tables 1 and 2 summarize the data used at these two airports.

Table 1. Total number of landings and landings used in the Inverse Model for data acquired at SFO.

| **Aircraft** | **Total Landings** | **Landings Used** |
|---|---|---|
| A319 | 88 | 81 |
| A320 | 175 | 168 |
| B732-735 | 534 | 520 |
| B738 | 131 | 121 |
| B747-400 | 173 | 164 |
| B757 | 480 | 462 |
| B767 | 226 | 215 |
| B777 | 100 | 95 |
| DC9 | 63 | 59 |
| **Total** | 1,970 | 1,885 |

Table 2. Total number of landings and landings used in the Inverse Model for data acquired at DEN.

| **Aircraft** | **Total Landings** | **Landings Used** |
|---|---|---|
| A319 | 1,464 | 854 |
| A320 | 648 | 384 |
| B732-735 | 783 | 408 |
| B738 | 379 | 210 |
| B747-400 | 24 | 16 |
| B757 | 603 | 422 |
| B767 | 70 | 50 |
| B777 | 89 | 63 |
| **Total** | 4,060 | 2,407 |

To be used in the Inverse Model, we required that data for each landing consists of at least three data points for both the port and starboard vortices. This criterion reduces the number of landings used in the Inverse Model to 1,885 at SFO, and 2,407 at DEN.

In addition to the above criterion, further restrictions on the DEN data were imposed in an earlier interim Inverse Model analysis (Lai et al., 2007c). However, in this Final Report, these restrictions were removed so that all the DEN data were used in the Inverse Model. Our analysis showed that there are only small differences with or without these restrictions.

The earlier restrictions are due to the concern over the large, unexpected Vo spread in the DEN lidar data. Figure 1 shows the frequency distributions (histograms) of $V_o$ estimates from the B733 (for B737-200 through 500 aircraft models) lidar data at SFO (top panel) and at DEN (bottom panel). The histograms at the two airports are drastically different. The $V_o$ estimates from the DEN data have a much larger spread than those from the SFO data. The presence of an updraft/downdraft and/or a stratified layer could result in vortex descent rates smaller or larger than expected under calm, unstratified environmental conditions. We hypothesize that updrafts, downdrafts, and stratified atmospheric layers are found more frequently at DEN than at SFO, arising both from convective and mountain flows conditions. These conditions result in the much larger spread in the apparent $V_o$ at DEN.

Since the phenomena that caused the anomalous $V_o$ at DEN are not included in the forward model SHRAPA, the inversion of data with these apparent $V_o$ would yield unrealistic results from the Inverse Model. Therefore, only the DEN lidar data with $V_o$ estimates within ± two standard deviations from the median $V_o$ observed at SFO were used in the Inverse Model in the interim analysis.

### 4.1 Examples of Results from the Wake Vortex Inverse Model

Several examples of realistic results from the wake vortex Inverse Model are shown: Figure 2 for a DC9 at MEM, Figure 3 for a B737-800 at SFO, and Figure 4 for a B737-300 at SFO. In each figure, the red and blue symbols and lines represent the observed data. The black lines (solid and dash) represent the Inverse Model results. The observed lateral and vertical positions of the vortices (shown in the two top panels) were used in the inversion. The Inverse Model results for the vortex circulation and crosswind vertical profile are shown in the bottom left and bottom right panels, respectively. Note that the observed circulation data and observed crosswind vertical profile (if available) were not used in the inversion; they are shown in this plot only for comparison with the Inverse Model results. The Inverse Model results for $b_o$, $\Gamma_o$ (labeled as $G_o$ in the figure), $y_o$ and $z_o$ are listed near the bottom of the figure.

In these examples, the Inverse Model followed the general trend of the observed vortex lateral and vertical positions and ignored the smaller fluctuations, as it is constrained to do. The model performed well both in a strong crosswind of 3 m/s (Figure

3) and in a weak crosswind (Figure 4). The model also performed well in a crosswind with a significant vertical gradient (Figure 2). In all three cases, the Inverse Model circulations compared favorably with the observed values.

Not all results from the Inverse Model appear to be realistic. The Inverse Model fails when the observed vortex lateral and vertical positions are manifestations of conditions that are not included in the forward model. We identify three scenarios for the failure of the Inverse Model: (1) the presence of a downdraft, (2) the presence of an updraft, and (3) inconsistent data.

Figure 5 shows a case of a vortex wake in a downdraft, indicated by an increase in the descent rate of the vortex over time (cf., the top right panel in Figure 5). The Inverse Model was able to follow the observed vortex lateral and vertical positions. However, since the forward model does not recognize a downdraft, the only way that the Inverse Model can increase the descent rate is to increase the vortex strength (circulation), as shown in the figure.

Figure 6 shows a case of a vortex wake in an updraft, indicated by the low initial value for $V_o$ of 1.16 m/s, shown in the bottom left text in the figure, as well as the decrease in the descent rate of the vortex over time. Again, the Inverse Model was able to follow the observed vortex lateral and vertical positions. However, since the forward model does not recognize an updraft, the only way that the Inverse Model can decrease the descent rate is to decrease the vortex strength, resulting in an unrealistic rapid decrease in the circulation.

Figure 7 shows an example of inconsistent observed data. The data show that the vortex pair became tilted over time, indicated by the port and starboard vortices having different lateral and vertical positions after the wake age of 30s. This tilt can also be visualized by examining the altitude versus lateral transport plot in the figure. The point vortex physics in SHRAPA implies that, if the vortex pair is tilted but with one vortex not exactly vertically above the other, the vortices must migrate vertically. When the vortices are tilted and one vortex is not exactly vertically above the other vortex, and the vortices are migrating horizontally but not vertically, as in Figure 7, the data are inconsistent with the model. In this case, the model tries to reduce the circulation, resulting in the unrealistic Inverse Model circulation results shown in the figure.

### 4.2 Vortex Circulation Comparison

The time histories of vortex circulation obtained by the Inverse Model were compared with a baseline dataset considered to be reliable. This baseline dataset consists mainly of the OGE vortex data at MEM, obtained using a CW lidar. Our baseline dataset consists of a total of 110 landings from five different aircraft models: A300, A320, B727, DC10, and DC9. The median of the normalized circulation data for each aircraft model are plotted against their normalized wake age as blue lines and symbols in Figure 8, where circulation is normalized by $\Gamma_o$ and the wake age is normalized by $b_o/V_o$. While there is scatter in the baseline dataset, the normalized data tend to follow a similar decay

rate. We will be comparing the median of the inversion circulation time histories to the baseline data shown in this figure.

CW lidar data from 29 B727 landings and 16 DC9 landings at MEM were used in the Inverse Model. The median normalized circulations from the inversion for the two aircraft models are superimposed on the baseline data in Figure 9. The median circulation for the B727 is slightly higher than the baseline data while the decay rate is very similar. The median circulation from the Inverse Model for the DC9 is noisy due to the limited amount of data, but the average decay rate is similar to the decay rate of the baseline data.

Pulsed lidar data for 9 aircraft models (A319, A320, B737-200 through 500, B738, B747-400, B757, B767, B777, and DC9) at SFO were also used in the Inverse Model. Data from a total of 1,885 landings were used. The median normalized circulations from the Inverse Model are plotted in red in Figure 10. Again, the Inverse Model results are within the scatter of the baseline data.

Inverse Model circulations for the DEN pulsed lidar data (shown in black) are shown in Figure 11, together with the SFO Inverse Model circulation and the baseline data. Pulsed lidar data for 8 aircraft models (A319, A320, B737-200 through 500, B738, B747-400, B757, B767, and B777) at DEN, representing data from 2,407 landings, were used in the inversion. The results from the Inverse Model using the DEN data are, again, in good agreement with the Inverse Model results from SFO and the baseline data, but appear to be slightly higher than the others for $\Gamma >\sim 4$.

### 4.3 Initial Vortex Separation Comparison

The initial horitontal vortex separation ($b_o$) is one of the vortex parameters estimated in the Inverse Model. The initial guess of $b_o$ used in the Inverse Model for each landing is provided by a database in which $b_o$ is computed from $V_o$ estimated from the time histories of the vertical position of the vortices (Lai and Delisi, 2007b). The $b_o$ at the end of an inversion run is the best-fit value based on the initial guess $b_o$, and the observed data (vertical and lateral positions) used in the Inverse Model. This section compares the $b_o$ from the $V_o$ database and the Inverse Model $b_o$.

Table 3 summarizes the medians of $b_o$ from the $V_o$ database and those from the Inverse Model for 9 aircraft models. Data from 4,308 landings were used in this table. The medians of the Inverse Model $b_o$ are consistently smaller than those computed from $V_o$. The maximum difference is about 3m for the B744 aircraft, while most of the differences are about 1m.

Table 3. Comparison of $b_o$ computed from $V_o$ estimates, and $b_o$ from the wake vortex Inverse Model. B733 includes aircraft models B737-200 through 500. B744 are for aircraft model B747-400.

| A/C | Landings Used | Span (m) | Elliptical $b_o$ (m) | Median $b_o$ (m) (from $V_o$) | Median $b_o$ (m) (from Inverse Model) |
|---|---|---|---|---|---|
| A319 SFO | 81 | 34.1 | 26.8 | 25.8 | 25.1 |
| DEN | 854 | | | 26.8 | 26.2 |
| A320 SFO | 168 | 34.1 | 26.8 | 25.3 | 24.6 |
| DEN | 384 | | | 24.8 | 24.4 |
| B733 SFO | 520 | 28.8 | 22.6 | 24.0 | 22.9 |
| DEN | 408 | | | 22.9 | 22.3 |
| B738 SFO | 121 | 34.3 | 26.9 | 25.1 | 24.0 |
| DEN | 210 | | | 25.7 | 24.9 |
| B744 SFO | 164 | 64.6 | 50.7 | 47.5 | 44.2 |
| DEN | 16 | | | 46.2 | 43.0 |
| B757 SFO | 462 | 38.0 | 29.8 | 32.7 | 31.1 |
| DEN | 422 | | | 32.0 | 30.3 |
| B767 SFO | 215 | 47.6 | 37.4 | 38.5 | 36.4 |
| DEN | 50 | | | 40.9 | 38.3 |
| B777 SFO | 95 | 60.9 | 47.8 | 38.4 | 37.0 |
| DEN | 63 | | | 38.4 | 37.7 |
| DC9 SFO | 59 | 28.4 | 22.3 | 25.5 | 24.4 |
| MEM | 16 | | | 27.1 | 26.3 |

The $b_o$ estimates in the $V_o$ database are determined solely from the observed time histories of the vertical positions, and, therefore, the vertical descent rate of the vortices (Lai and Delisi, 2007b). The $b_o$ computed from the Inverse Model are determined by a combination of the initial guess of $b_o$ and the observed vertical and lateral separations of the vortices. Past studies (Gulsrud and Wang, 2005) have shown that $b_o$ computed from vertical and lateral vortex separations (by differencing the observed lateral and vertical positions of the port and starboard vortices) are smaller than those shown in Table 3. We duplicated the analysis of Gulsrud and Wang (2005) using pulsed lidar data at SFO for 3 aircraft models (B737-200 through 500, B747-400, and B777). The resulting median $b_o$ are 20.7, 40.1 and 34.9m, respectively for the 3 aircraft models. All three estimates are indeed smaller than the corresponding $b_o$ medians shown in Table 3 from either method.

The uncertainty in a lidar vortex core position measurement is 6.5m in the lateral (spanwise) direction and 4.5m in the vertical direction (Laporte, 2006). Thus, when estimating the lateral distance between two vortex cores, the uncertainty is the square root

of two times 6.5m, or 9.2m. This uncertainty is large relative to $b_o$ for many aircraft, e.g., if $b_o$ is 24.0m for a B733 aircraft (cf., Table 3), the uncertainty in estimating the distance between two vortex cores is 38% of $b_o$. Since the uncertainty in the vertical positions is less than half the uncertainty in estimating $b_o$ from the vortex core lateral positions, we hypothesize that the $b_o$ estimated from $V_o$ are more accurate than those estimated from the lidar vortex lateral position data.

Also, from Table 3, Gulsrud and Wang (2005), and the analysis above, the median $b_o$ from $V_o$ are larger than the $b_o$ estimated using the lidar vortex core positions. Thus, it appears that, relative to $b_o$ estimates from $V_o$, there is a bias towards smaller values of $b_o$ estimated using the lidar vortex core positions. Since the results from the Inverse Model are a "best fit" to the lidar lateral and vertical vortex core position data, it follows that the $b_o$ estimates from the Inverse Model will be smaller than the $b_o$ from $V_o$ estimates. As noted above, we see in Table 3 smaller values of $b_o$ from the Inverse Model than the $b_o$ from $V_o$ estimates.

Given the above analyses, we believe that the $b_o$ estimated from $V_o$ yield the most accurate estimates of $b_o$ and that $b_o$ estimated by subtracting the lateral distance between the two vortex cores gives the least accurate estimates of $b_o$.

## 5. Summary

An Inverse Model for inverting landing aircraft wake vortex position data has been developed at NWRA. The model uses time history measurements of the lateral and vertical position of aircraft vortices to obtain estimates of initial vortex separation, the vortex circulation decay, and the crosswind vertical profile. This Inverse Model was applied to OGE lidar data from more than 4,000 aircraft landings at MEM, SFO and DEN airports.

The median normalized circulations for different aircraft models estimated from the Inverse Model are consistent with what we believe is a reliable baseline of observed data. This consistency suggests that a single normalized circulation decay rate can be used for modeling the median decay of vortices in the OGE region.

From our analysis and the errors in lidar vortex core position estimated by Laporte (2006), we believe that estimates of the initial horizontal spacing of the vortices, $b_o$, using the initial vortex descent velocity, $V_o$, yield the most accurate estimates and that $b_o$ estimates obtained by subtracting the lidar-estimated distance between the two vortices yields the least accurate estimates of $b_o$.

## References


Greene, G. C., 1986. An Approximate Model of Vortex Decay in the Atmosphere. Journal of Aircraft, Vol. 23, No. 7, pp. 566-573.

Gulsrud, A. and F.Y. Wang, 2005. OGE Vortex Spacing Statistics from SFO (2001 and DIA (2003). Presentation at the Volpe Center, September 21, 2005.

Lai, D.Y. and D.P. Delisi, 2007a. Wake Vortex Inverse Model User's Guide. NorthWest Research Associates Technical Report NWRA-Bell-07-R351.

Lai, D.Y. and D.P. Delisi, 2007b. Preliminary Estimates of the Initial Aircraft Vortex Separation. NorthWest Research Associates Technical Report NWRA-Bell-07-R354.

Lai, D.Y., G.R. Mellman, R.E. Robins and D.P. Delisi, 2007c. Wake Vortex Inverse Model and its Validation. NorthWest Research Associates Technical Report NWRA-Bell-07-R359.

Laporte, F., 2006. E-mail to the A380 Wake Vortex Working Group, Subject: Status of Airbus Actions from the A380 Wake Vortex Bremen/Sevilla Meetings, 13 April 2006.

Robins, R.E. and D.P. Delisi, 2006. Modeling Crosswind Shear Effects in NASA's AVOSS Prediction Algorithm. AIAA Paper 2006-1076, 44th Aerospace Sciences Meeting, Reno NV, January 9-12.

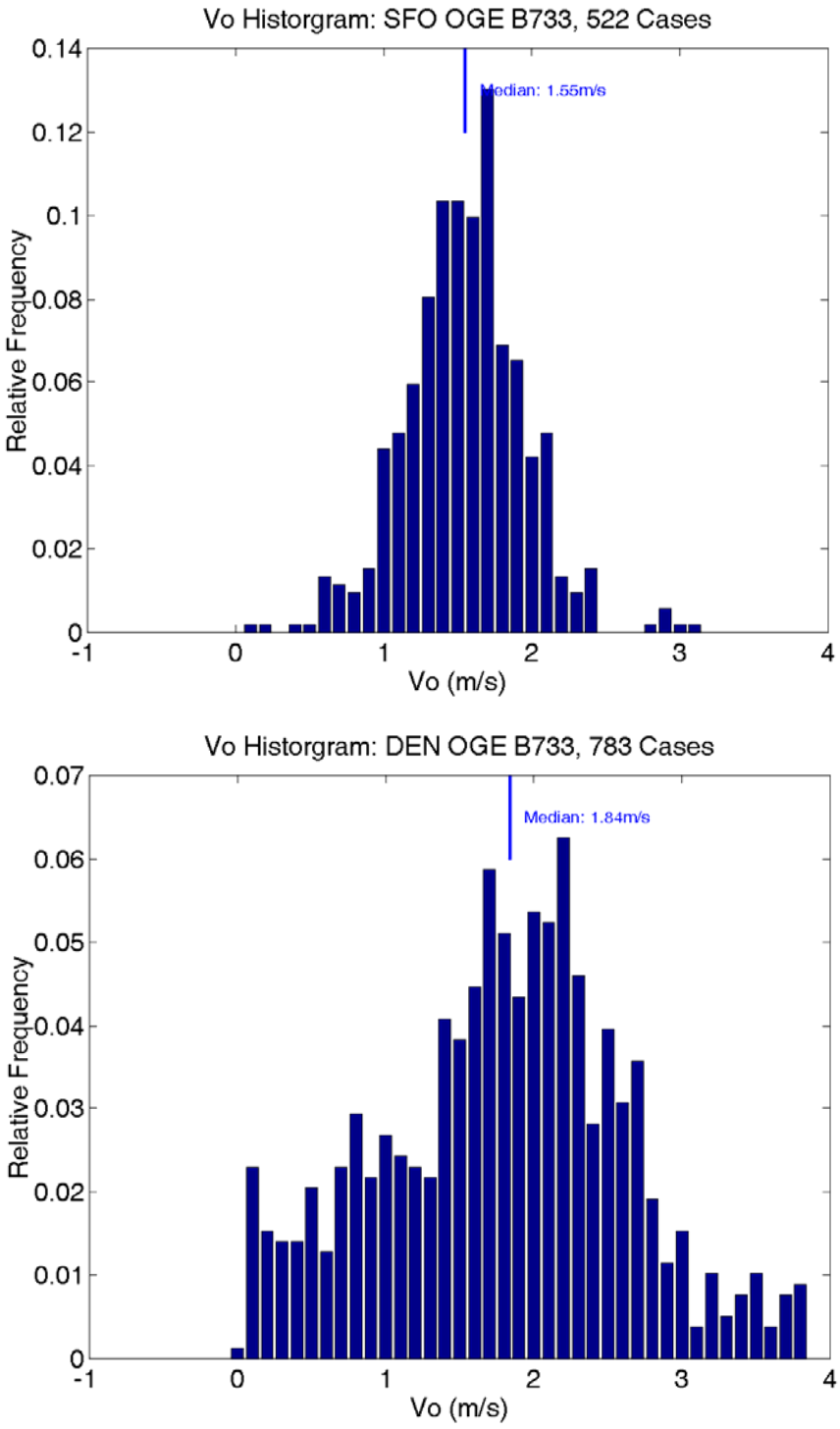


Figure 1. Histograms of $V_o$ estimated by performing linear regressions using the time series of observed vertical positions of vortices for B737-200 through 500 aircraft models at SFO (top panel) and DEN (bottom panel). The numbers of landings listed in these two figures are different from those used in the Inverse Model (Tables 1 and 2) due to the criteria used in selecting data for the inverse modeling.

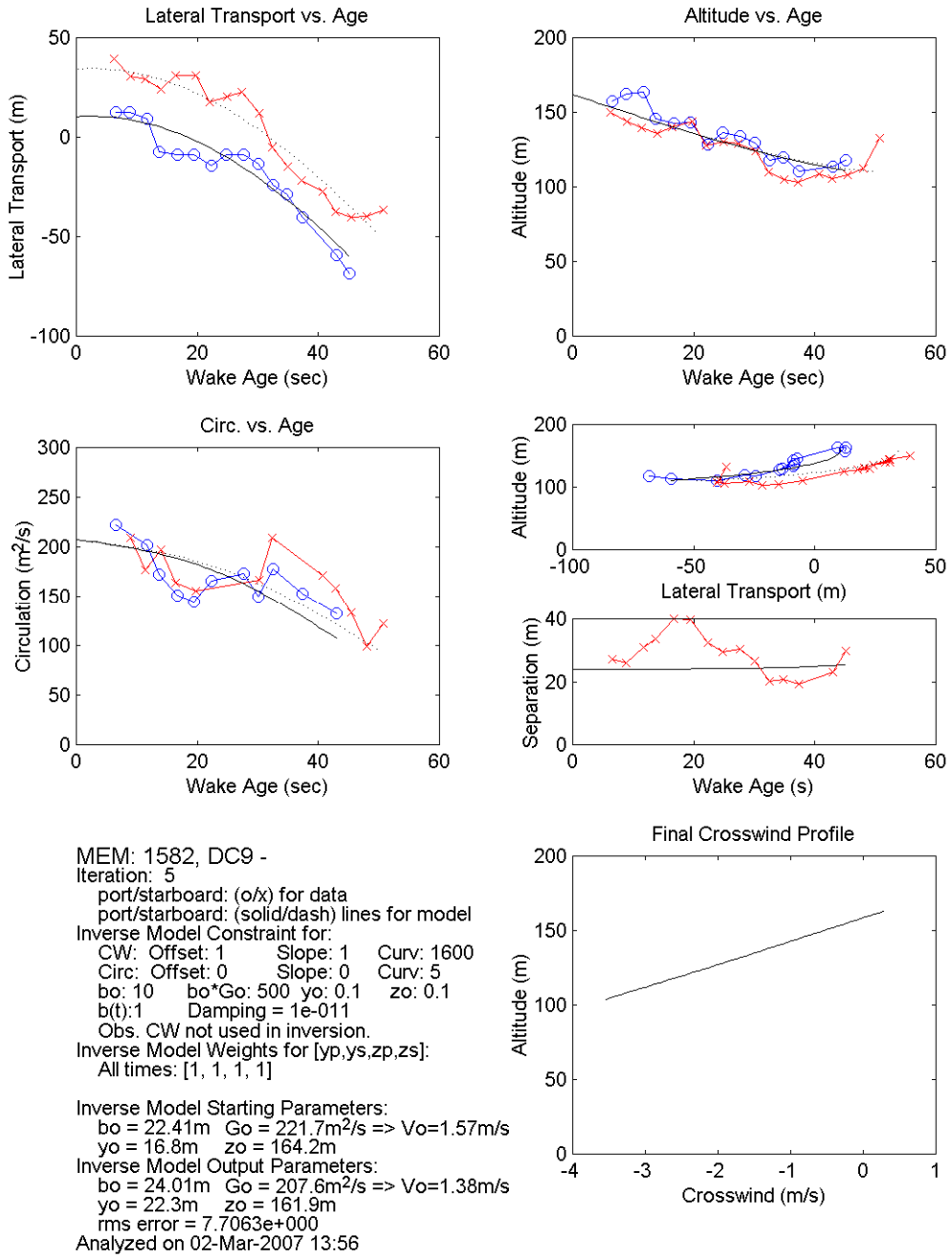


Figure 2. Example of realistic wake vortex Inverse Model results for a DC9 at MEM. The red and blue symbols and lines represent data observed using a CW lidar. The black lines represent results from the Inverse Model. The observed lateral and vertical positions of the vortices were used in the Inverse Model. Note that the observed circulation data were not used in the Inverse Model, but are presented in this plot for comparison with the circulations obtained from the model.

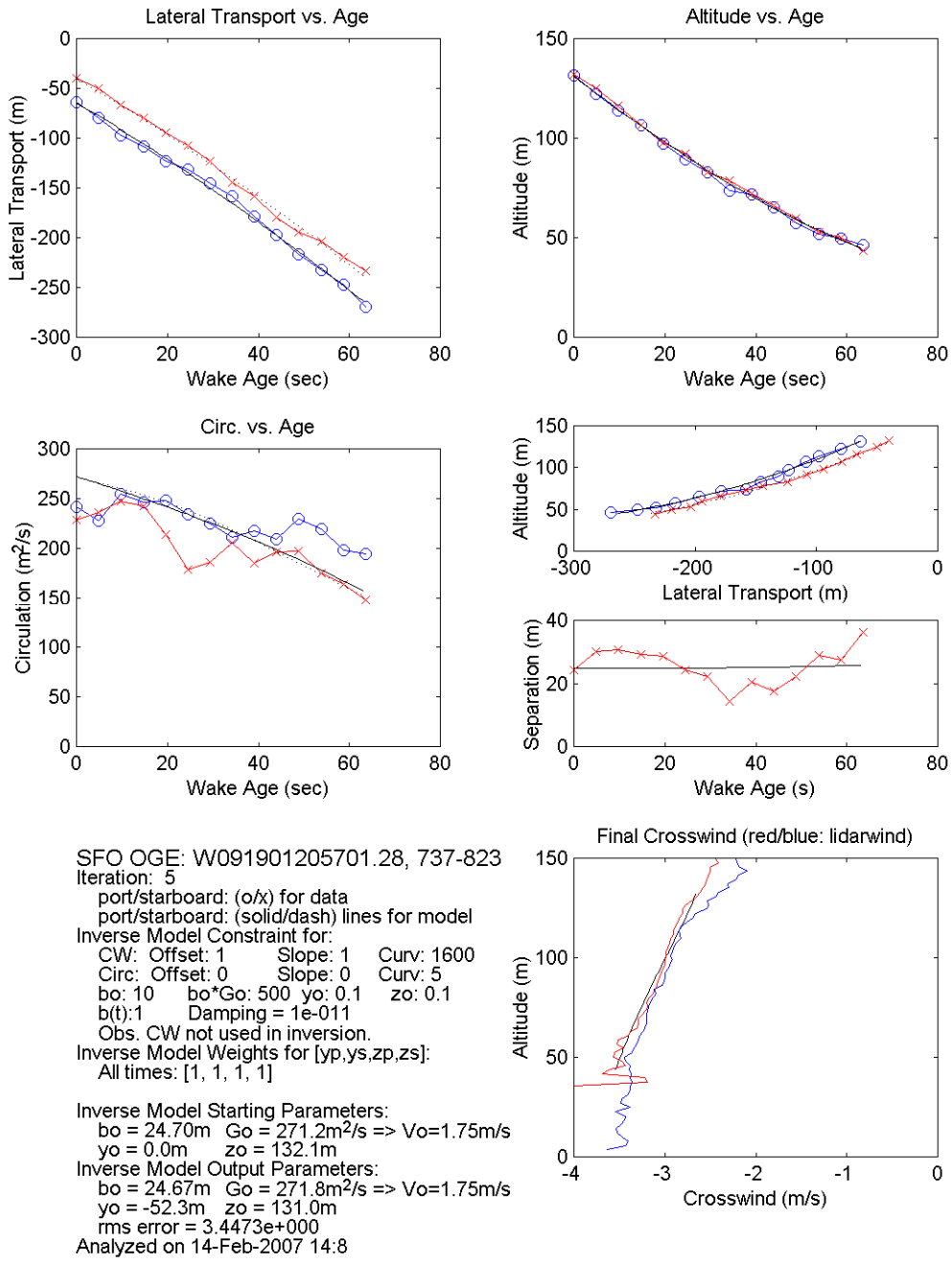


Figure 3. Example of realistic wake vortex Inversion Model results for a B737-800 at SFO. The red and blue symbols and lines represent data observed using a pulsed lidar. The black lines represent results from the Inverse Model. The observed lateral and vertical positions of the vortices were used in the Inverse Model. Note that the observed circulation data and crosswind profile were not used in the Inverse Model, but are presented in this plot for comparison with the circulations and crosswind profile obtained from the model.

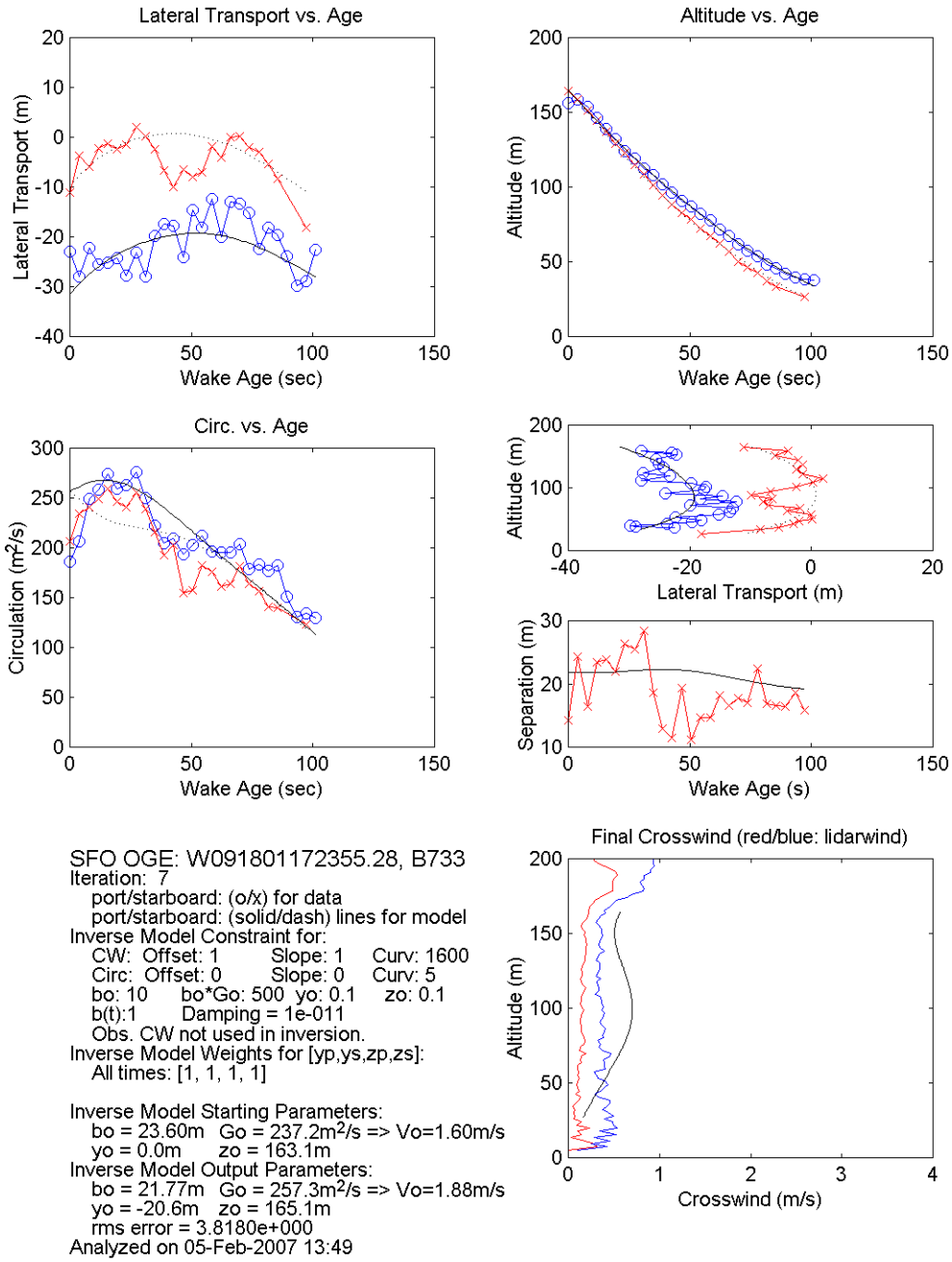


Figure 4. Example of realistic wake vortex Inverse Model results for a B737-300 at SFO. The red and blue symbols and lines represent data observed using a pulsed lidar. The black lines represent results from the Inverse Model. The observed lateral and vertical positions of the vortices were used in the Inverse Model. Note that the observed circulation data and crosswind l profile were not used in the Inverse Model, but are presented in this plot for comparison with the circulations and crosswind profile obtained from the model.

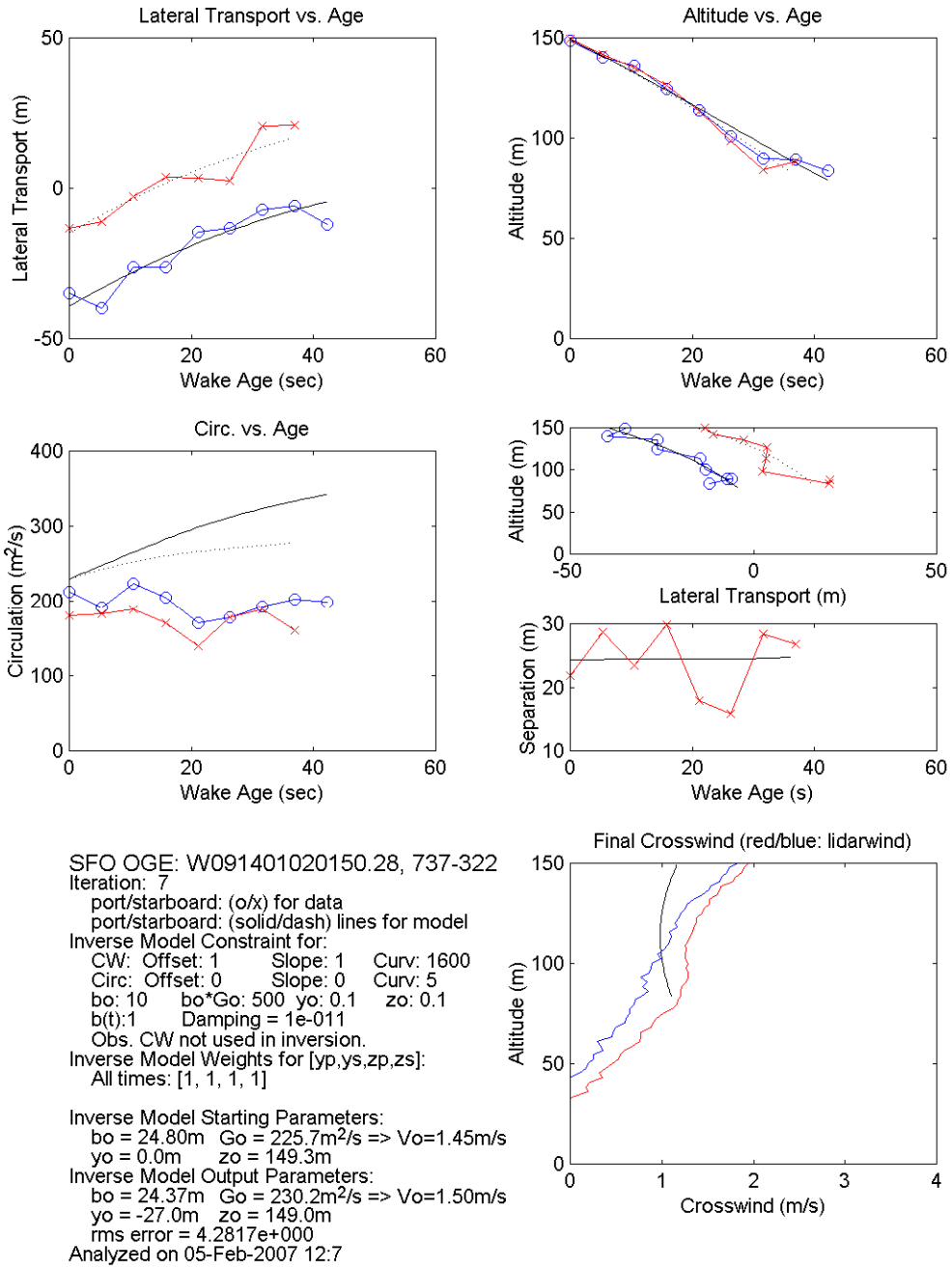


Figure 5. Example of Inverse Model results with a wake vortex in a downdraft. The red and blue symbols and lines represent data observed using a pulsed lidar. The black lines represent results from the Inverse Model. The observed lateral and vertical positions of the vortices were used in the Inverse Model. Note that the observed circulation data and crosswind vertical profile were not used in the Inverse Model, but are presented in this plot for comparison with the circulations and crosswind profile obtained from the model.

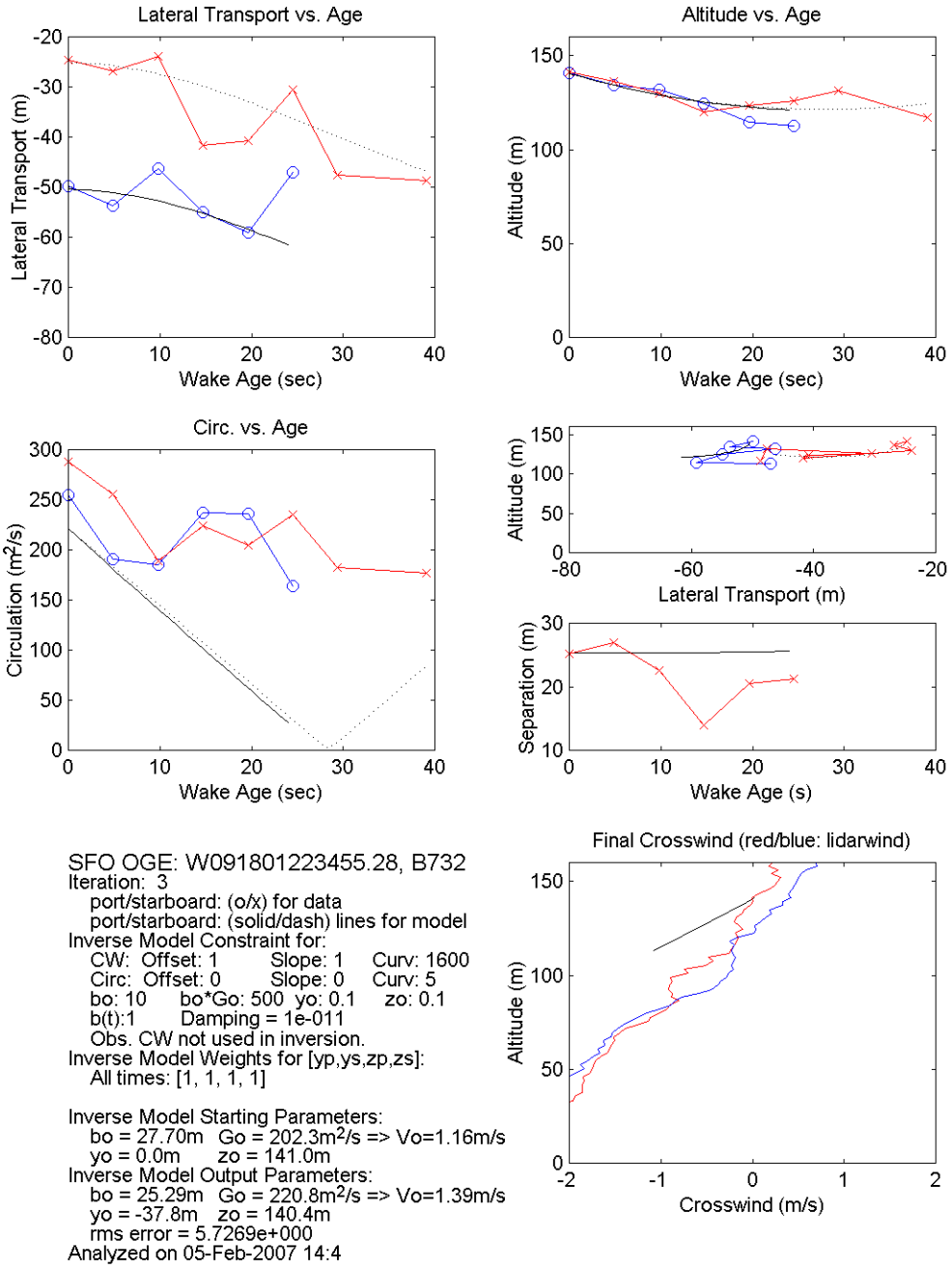


Figure 6. Example of Inverse Model results with a wake vortex in an updraft. The red and blue symbols and lines represent data observed using a pulsed lidar. The black lines represent results from the Inverse Model. The observed lateral and vertical positions of the vortices were used in the Inverse Model. Note that the observed circulation data and crosswind vertical profile were not used in the Inverse Model, but are presented in this plot for comparison with the circulations and crosswind profile obtained from the model.

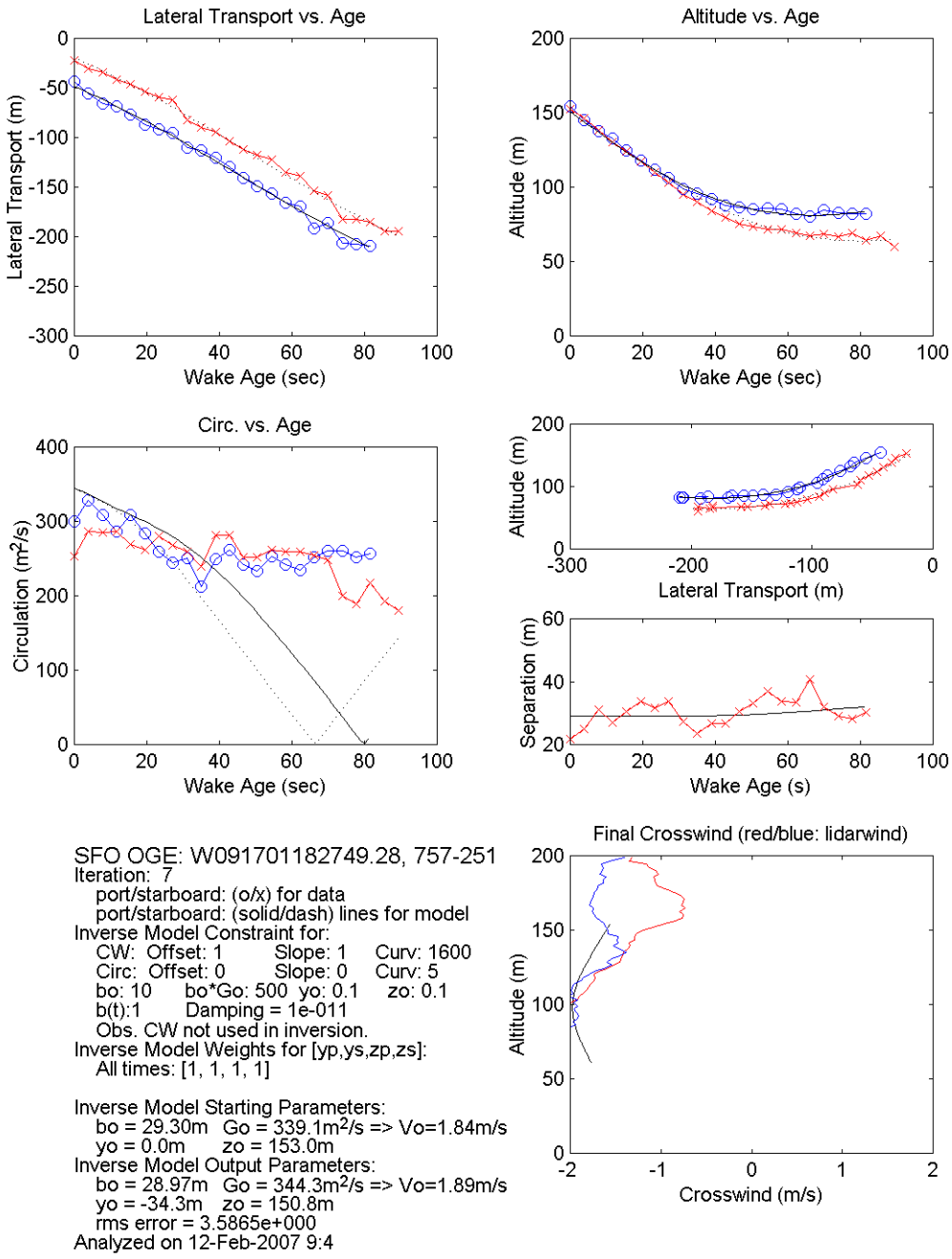


Figure 7. Example of Inverse Model results with a wake vortex with inconsistent data. The red and blue symbols and lines represent data observed using a pulsed lidar. The black lines represent results from the Inverse Model. The observed lateral and vertical positions of the vortices were used in the Inverse Model. Note that the observed circulation data and crosswind vertical profile were not used in the Inverse Model, but are presented in this plot for comparison with the circulations and crosswind profile obtained from the model.

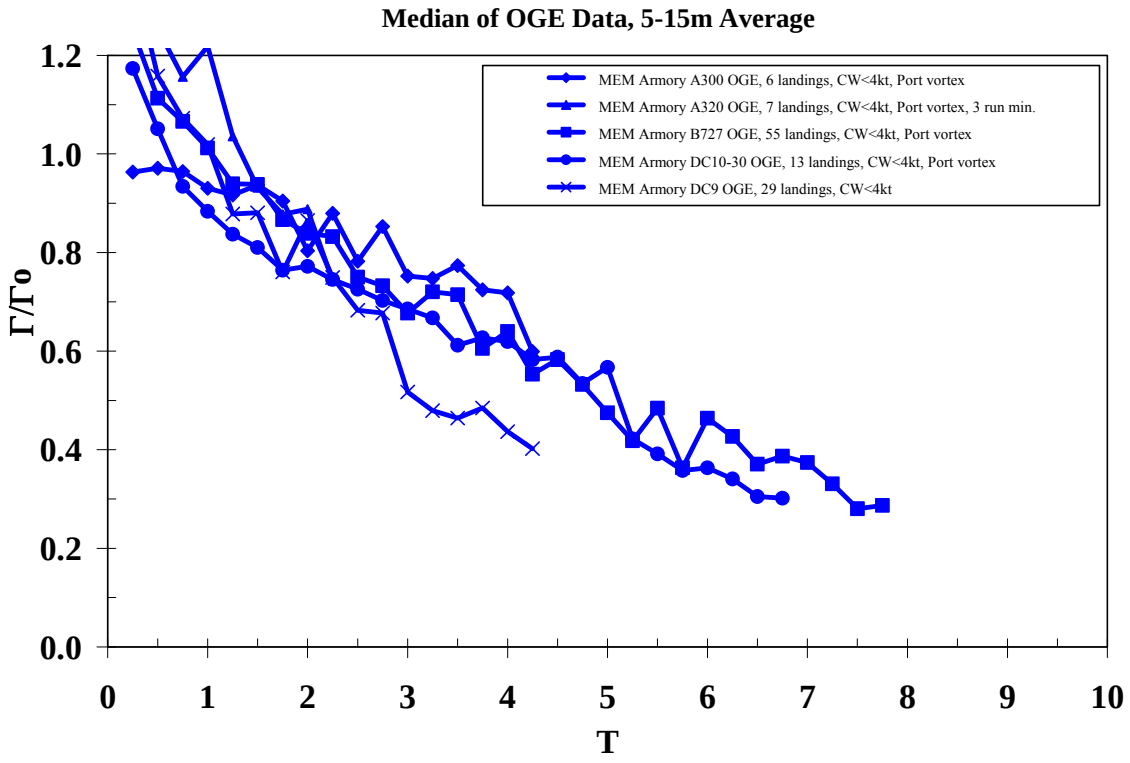


Figure 8. Baseline OGE circulation data used for validation of the Inverse Model results. Normalized median circulation for different aircraft models are plotted against their normalized wake age. The blue lines and symbols represent CW lidar data at MEM. Data from 110 landings were used in this figure.

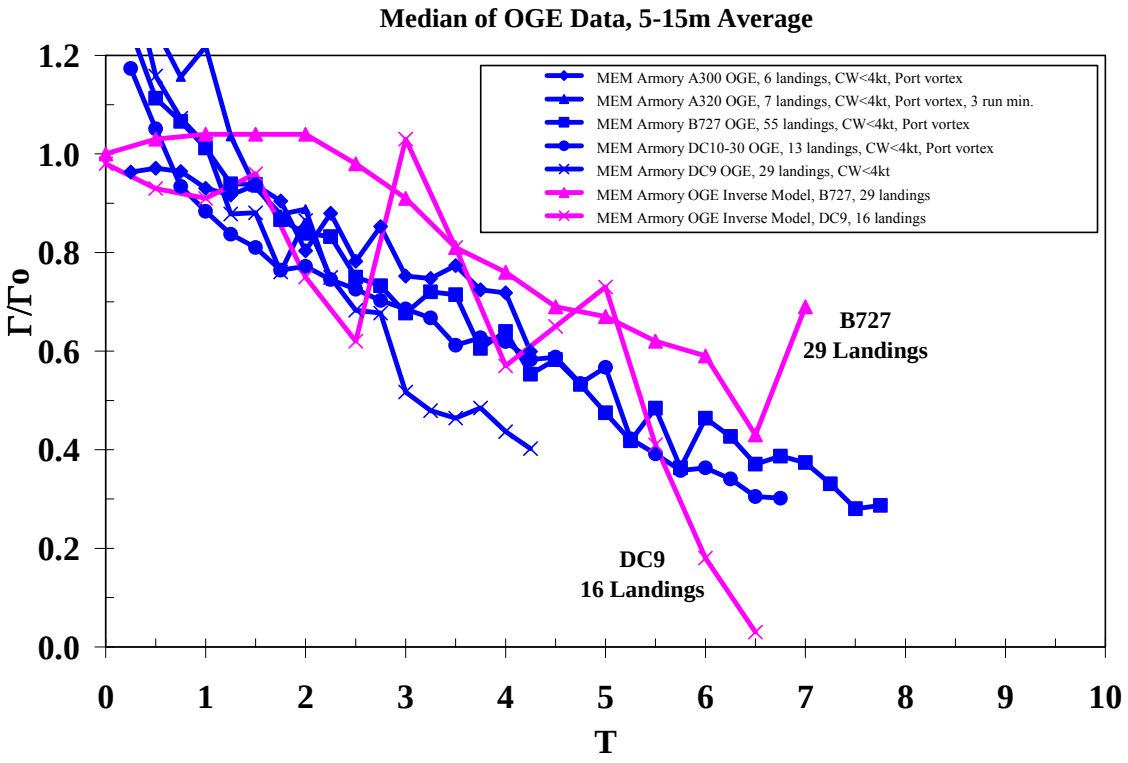


Figure 9. Comparison between the baseline data and the normalized Inverse Model circulations for the B727 and DC9 CW lidar data at MEM. The Inverse Model circulations are shown in magenta, and the baseline data in blue. A total of 29 B727 and 16 DC9 landings were used in the Inverse Model.

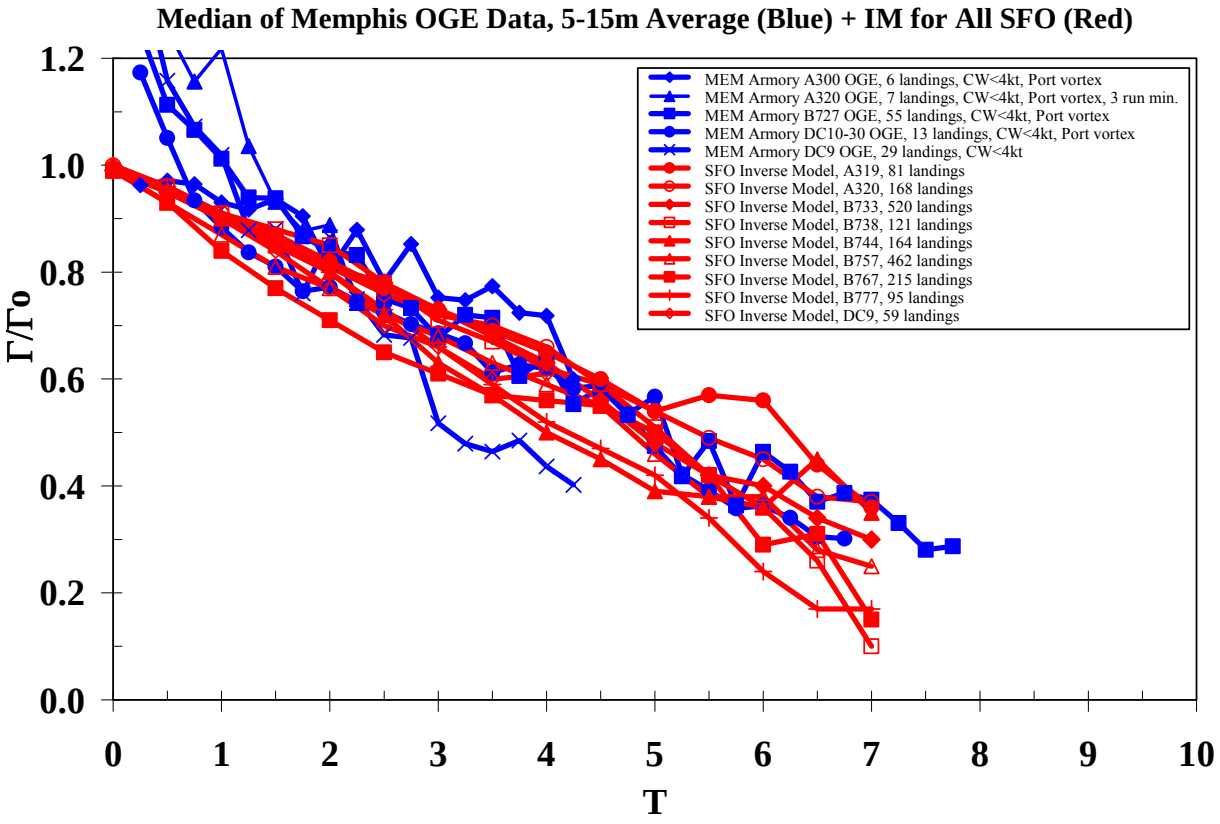


Figure 10. Comparison between the baseline data and the normalized Inverse Model circulation for 9 aircraft models at SFO. The Inverse Model circulations are shown in red, and the baseline data in blue. Pulsed lidar data for 9 aircraft models (A319, A320, B737-200 through 500, B738, B747-400, B757, B767, B777, and DC9) were used in the inversion. A total of 1,885 landings were used in the Inverse Model.

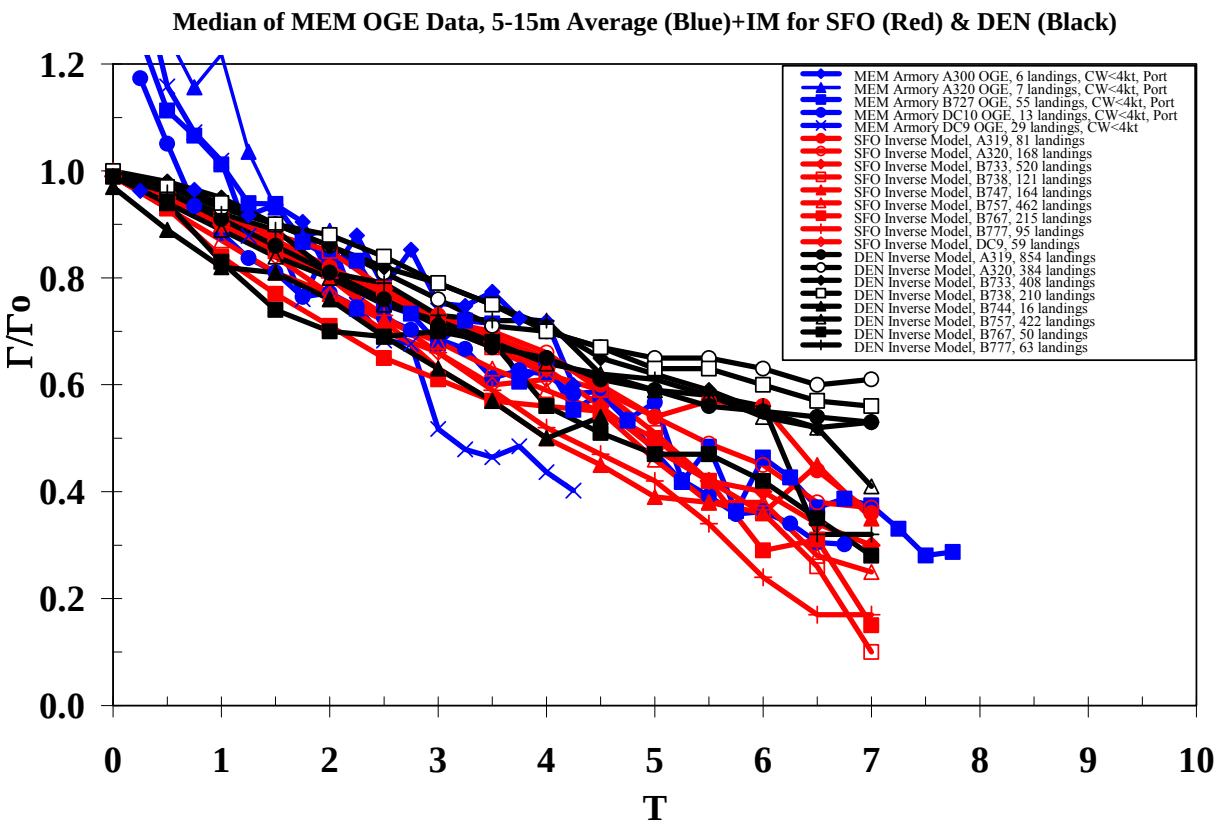


Figure 11. Comparison between the baseline data and the normalized Inverse Model circulation for 8 aircraft models at DEN, and 9 aircraft models at SFO. The baseline data are shown in blue and the Inverse Model circulations at SFO and DEN are shown in red and black, respectively. The 8 aircraft models for DEN are A319, A320, B737-200 through 500, B738, B747-400, B757, B767, and B777, constituting data from 2,407 landings.